

Impact of semi-annihilations on dark matter phenomenology – an example of Z_N symmetric scalar dark matter

G. Bélanger¹, K. Kannike^{2,3}, A. Pukhov⁴, M. Raidal³

September 18, 2018

¹ LAPTH, Univ. de Savoie, CNRS, B.P.110, F-74941 Annecy-le-Vieux Cedex, France

² Scuola Normale Superiore and INFN, Piazza dei Cavalieri 7, 56126 Pisa, Italy

³ National Institute of Chemical Physics and Biophysics, Rāvala 10, Tallinn 10143, Estonia

⁴ Skobeltsyn Inst. of Nuclear Physics, Moscow State Univ., Moscow 119992, Russia

Abstract

We study the impact of semi-annihilations $x_i x_j \leftrightarrow x_k X$, where x_i is any dark matter and X is any standard model particle, on dark matter phenomenology. We formulate minimal scalar dark matter models with an extra doublet and a complex singlet that predict non-trivial dark matter phenomenology with semi-annihilation processes for different discrete Abelian symmetries Z_N , $N > 2$. We implement two such example models with Z_3 and Z_4 symmetry in micrOMEGAs and work out their phenomenology. We show that both semi-annihilations and annihilations involving only particles from two different dark matter sectors significantly modify the dark matter relic abundance in this type of models. We also study the possibility of dark matter direct detection in XENON100 in those models.

1 INTRODUCTION

The origin of dark matter of the Universe is not known. In popular models with new particles beyond the standard model particle content, such as the minimal supersymmetric standard model, an additional discrete Z_2 symmetry is introduced [1]. As a result, the lightest new Z_2 -odd particle, x , is stable and is a good candidate for dark matter. The phenomenology of this type of models has been studied extensively.

The discrete symmetry that stabilises dark matter must be the discrete remnant of a broken gauge group [2], because global discrete symmetries are broken by gravity. The most natural way for the discrete symmetry to arise is from the breaking of a $U(1)_X$ embedded in a larger gauge group, e.g. $SO(10)$ [3]. The latter contains gauged $B - L$ as a part of the symmetry, and the existence of dark matter can be related to the neutrino masses, leptogenesis and, in a broader context, to the existence of leptonic and baryonic matter [4–6].

Obviously, the discrete remnant of $U(1)_X$ need not to be Z_2 – in general it can be any Z_N Abelian symmetry. The possibility that dark matter may exist due to Z_N , $N > 2$, is a known [7–15], but much less studied scenario.¹ Model independently, it has been pointed out in Ref. [15] that in Z_N models the dark matter annihilation processes contain new topologies with different number of dark matter particles in the initial and final states – called semi-annihilations –, for example $xx \leftrightarrow x^* X$, where X can be any standard model particle. It has been argued that those processes may significantly change the predictions for the dark matter relic abundance in thermal freeze-out. Furthermore, an

¹Phenomenology of Z_3 -symmetric dark matter in supersymmetric models has been studied in Refs. [7,10] and in extra dimensional models in Refs. [8,9].

enlarged discrete symmetry group makes it possible to have more than one dark matter candidate. In this case, annihilation processes involving only particles from the dark sectors, leading to the assisted freeze-out mechanism, can also influence the relic abundance of both dark matter candidates [16,17]. The assisted freeze-out mechanism in the case of a $Z_2 \times Z_2$ symmetry was discussed in [17]. However, no detailed studies have been performed that compare dark matter phenomenology of different Z_N models. This is difficult also because presently the publicly available tools for computing dark matter relic abundance do not include the possibility of imposing a Z_N discrete symmetry instead of a Z_2 .

The aim of this work is to formulate the minimal scalar dark matter model that predicts different non-trivial scalar potentials for different Z_N symmetries and to study their phenomenology. In particular we are interested in quantifying the possible effects of semi-annihilation processes $xx \leftrightarrow x^*X$ as well as of annihilation processes involving particles from two different dark sectors on generating the dark matter relic abundance. In order to perform quantitatively precise analyses we implement minimal Z_3 and Z_4 symmetric scalar dark matter models that contain one singlet and one extra doublet in micrOMEGAs [18,19]. Using this tool we show that, indeed, the semi-annihilations and the annihilations between two dark sectors affect the dark matter phenomenology and should be taken into account in a quantitatively precise way in studies of any particular model.

2 Z_N LAGRANGIANS

2.1 Z_N symmetry

Under an Abelian Z_N symmetry, where N is a positive integer, addition of charges is modulo N . Thus the possible values of Z_N charges can be taken to be $0, 1, \dots, N-1$ without loss of generality. A field ϕ with Z_N charge X transforms under a Z_N transformation as $\phi \rightarrow \omega^X \phi$, where $\omega^N = 1$, that is $\omega = \exp(i2\pi/N)$.

A Z_N symmetry can arise as a discrete gauge symmetry from breaking a $U(1)_X$ gauge group with a scalar, whose X -charge is N [2,4]. For larger values of N , the conditions the Z_N symmetry imposes on the Lagrangian approximate the original $U(1)$ symmetry for two reasons. First, assuming renormalisability, the number of possible Lagrangian terms is limited and will be exhausted for some small finite N , though they may come up in different combinations for different values of N . Second, if the Z_N symmetry arises from some $U(1)_X$, the X -charges of particles cannot be arbitrarily large, because that would make the model nonperturbative. If N is larger than the largest charge in the model, the restrictions on the Lagrangian are the same as in the unbroken $U(1)$.

We shall see below that in spite of the large number of possible assignments of Z_N charges to the fields, the number of possible distinct potentials is much smaller.

2.2 Field content of the minimal model

In order to study the impact of different discrete Z_N symmetries on dark matter phenomenology, the example model must contain more than one neutral particle in the dark sector. The minimal dark matter model with such properties contains, in addition to the standard model fermions and the standard model Higgs boson H_1 , one extra scalar doublet H_2 and one extra complex scalar singlet S [5]. In the case of Z_2 symmetry, as proposed in [5], those new fields can be identified with the well known inert doublet H_2 [20–23] and the complex singlet S [24–28]. The phenomenology of those models is well studied. However, when both the doublet and singlet are taken into account, qualitatively new features concerning dark matter phenomenology, electroweak symmetry breaking and collider phenomenology occur [5,6,29–31]. The field content of the minimal scalar Z_N model is summarised in Table 1.

Table 1: Scalar field content of the low energy theory with the components of the standard model Higgs H_1 in the Feynman gauge. The value of the Higgs VEV is $v = 246$ GeV.

Field	$SU(3)$	$SU(2)_L$	T^3	$Y/2$	$Q = T^3 + Y/2$
$H_1 = \begin{pmatrix} G^+ \\ \frac{v+h+iG^0}{\sqrt{2}} \end{pmatrix}$	1	2	$\begin{pmatrix} \frac{1}{2} \\ -\frac{1}{2} \end{pmatrix}$	$\frac{1}{2}$	$\begin{pmatrix} 1 \\ 0 \end{pmatrix}$
$H_2 = \begin{pmatrix} -iH^+ \\ \frac{H^0+iA^0}{\sqrt{2}} \end{pmatrix}$	1	2	$\begin{pmatrix} \frac{1}{2} \\ -\frac{1}{2} \end{pmatrix}$	$\frac{1}{2}$	$\begin{pmatrix} 1 \\ 0 \end{pmatrix}$
$S = \frac{S_H+iS_A}{\sqrt{2}}$	1	1	0	0	0

2.3 Constraints on charge assignments

The assignments of Z_N charges have to satisfy

$$\begin{aligned}
X_S &> 0, \\
X_1 &\neq X_2, \\
-X_\ell + X_1 + X_e &= 0 \pmod{N}, \\
-X_q + X_1 + X_d &= 0 \pmod{N}, \\
-X_q - X_1 + X_u &= 0 \pmod{N}.
\end{aligned} \tag{1}$$

The first and second conditions arise from avoiding the $|H_1|^2 S$ term and Yukawa terms for H_2 , respectively, and the rest from requiring Yukawa interactions between H_1 and standard model fermions. The choice of Z_N charges for standard model fermions, the standard model Higgs H_1 , the inert doublet H_2 and the complex singlet S must be such that there are no Yukawa terms for H_2 and no mixing between H_1 and H_2 : only annihilation and semi-annihilation terms for H_2 and S are allowed. While we will see below that there are many assignments that satisfy Eq. (1), in each case it was possible to find an assignment with the charges of standard model fields set to zero: $X_{q,\ell,u,d,e,1} = 0$.

All possible scalar potentials contain a common piece because the terms where each field is in pair with its Hermitian conjugate are allowed under any Z_N and charge assignment. We denote it by V_c (the ‘c’ stands for ‘common’):

$$\begin{aligned}
V_c &= \lambda_1 \left(|H_1|^2 - \frac{v^2}{2} \right)^2 + \mu_2^2 |H_2|^2 + \lambda_2 |H_2|^4 + \mu_S^2 |S|^2 + \lambda_S |S|^4 \\
&+ \lambda_{S1} |S|^2 |H_1|^2 + \lambda_{S2} |S|^2 |H_2|^2 + \lambda_3 |H_1|^2 |H_2|^2 + \lambda_4 (H_1^\dagger H_2)(H_2^\dagger H_1).
\end{aligned} \tag{2}$$

2.4 The Z_2 scalar potential

There are 256 ways to assign the possible Z_2 charges 0, 1 to the standard model and dark sector fields. Of these, 8 satisfy Eq. (1); among them, there are 2 different assignments to the dark sector fields:

$X_S = X_1 = 1, X_2 = 0$ and $X_1 = 0, X_2 = X_S = 1$. Both give rise to the unique scalar potential

$$\begin{aligned}
V = V_c &+ \frac{\mu_S^2}{2}(S^2 + S^{\dagger 2}) + \frac{\lambda_5}{2} \left[(H_1^\dagger H_2)^2 + (H_2^\dagger H_1)^2 \right] \\
&+ \frac{\mu_{SH}}{2}(S^\dagger H_1^\dagger H_2 + S H_2^\dagger H_1) + \frac{\mu'_{SH}}{2}(S H_1^\dagger H_2 + S^\dagger H_2^\dagger H_1) \\
&+ \frac{\lambda'_S}{2}(S^4 + S^{\dagger 4}) + \frac{\lambda''_S}{2}|S|^2(S^2 + S^{\dagger 2}) \\
&+ \frac{\lambda'_{S1}}{2}|H_1|^2(S^2 + S^{\dagger 2}) + \frac{\lambda'_{S2}}{2}|H_2|^2(S^2 + S^{\dagger 2}).
\end{aligned} \tag{3}$$

2.5 Z_3 scalar potentials and particle content

There are 6561 ways to assign 0, 1, 2 to the fields. Of these, 108 satisfy Eq. (1); among them, there are 12 different assignments to the dark sector fields, giving rise to 2 different scalar potentials. The example potential we choose to work with (given by e.g. $X_1 = 0, X_2 = X_S = 1$) is

$$\begin{aligned}
V_{Z_3} = V_c &+ \frac{\mu''_S}{2}(S^3 + S^{\dagger 3}) + \frac{\lambda_{S12}}{2}(S^2 H_1^\dagger H_2 + S^{\dagger 2} H_2^\dagger H_1) \\
&+ \frac{\mu_{SH}}{2}(S H_2^\dagger H_1 + S^\dagger H_1^\dagger H_2),
\end{aligned} \tag{4}$$

which induces the semi-annihilation processes we are interested in. The second one is obtained from Eq. (4) by changing $S \rightarrow S^\dagger$ (with $\mu_{SH} \rightarrow \mu'_{SH}$ and $\lambda_{S12} \rightarrow \lambda_{S21}$).

The following conditions are sufficient to have the global minimum of potential at electroweak vacuum with $\langle S \rangle = 0, \langle H_2 \rangle = 0$:

$$\lambda_1, \lambda_2, \lambda_S, \lambda_{S1}, \lambda_{S2} > 0, \tag{5}$$

$$\lambda_3 + \lambda_4 > 0, \tag{6}$$

$$4\lambda_{S1}\lambda_{S2} > \lambda_{S12}^2, \tag{7}$$

$$\frac{\mu''^2}{\lambda_S} + \frac{\mu_{SH}^2}{\lambda_3 + \lambda_4} < 4\mu_S^2. \tag{8}$$

We use these conditions for our benchmark points.

The last term in Eq. (4) induces a mixing between the down component of H_2 and S . In terms of the mass eigenstates x_1, x_2 , we have

$$H_2 = \begin{pmatrix} -iH^+ \\ x_1 \sin \theta + x_2 \cos \theta \end{pmatrix}, \quad S = x_1 \cos \theta - x_2 \sin \theta. \tag{9}$$

The dark sector of this model consists of 3 complex particles x_1, x_2 , and H^+ with the Z_3 charge of 1. Taking the masses of x_1, x_2 and the mixing angle θ as free parameters of the model, we get the following relations

$$\mu_S^2 = M_{x_2}^2 \sin^2 \theta + M_{x_1}^2 \cos^2 \theta - \lambda_{S1} \frac{v^2}{2}, \tag{10}$$

$$\mu_{SH} = -4(M_{x_2}^2 - M_{x_1}^2) \frac{\cos \theta \sin \theta}{\sqrt{2}v}, \tag{11}$$

$$\mu_2^2 = -(\lambda_4 + \lambda_3) \frac{v^2}{2} + M_{x_1}^2 \sin^2 \theta + M_{x_2}^2 \cos^2 \theta. \tag{12}$$

The λ_1 and the mass of H^+ can be presented by formulas

$$\lambda_1 = \frac{1}{2} \frac{M_h^2}{v^2}, \tag{13}$$

$$M_{H^+} = \sqrt{\mu_2^2 + \lambda_3 \frac{v^2}{2}}. \tag{14}$$

where M_h is mass of SM Higgs.

2.6 Z_4 scalar potentials and particle content

There are 65536 ways to assign 0, 1, 2, 3 to the fields. Of these, 576 satisfy Eq. (1); among them, there are 36 different assignments to the dark sector fields, giving rise to 5 different scalar potentials. Among those the only potential that contains semi-annihilation terms is

$$V_{Z_4}^1 = V_c + \frac{\lambda'_S}{2}(S^4 + S^{\dagger 4}) + \frac{\lambda_5}{2} \left[(H_1^\dagger H_2)^2 + (H_2^\dagger H_1)^2 \right] \\ + \frac{\lambda_{S12}}{2}(S^2 H_1^\dagger H_2 + S^{\dagger 2} H_2^\dagger H_1) + \frac{\lambda_{S21}}{2}(S^2 H_2^\dagger H_1 + S^{\dagger 2} H_1^\dagger H_2), \quad (15)$$

invariant under e.g. the assignment of Z_4 charges $X_1 = 0, X_2 = 2, X_S = 1$.

The following conditions are sufficient to have global minimum of potential at electroweak vacuum with $\langle S \rangle = 0, \langle H_2 \rangle = 0$:

$$\lambda_1, \lambda_2, \lambda_{S1}, \lambda_{S2} > 0, \quad (16)$$

$$\lambda_S - |\lambda'_S| \geq 0, \quad (17)$$

$$\lambda_3 + \lambda_4 - |\lambda_5| > 0, \quad (18)$$

$$(|\lambda_{S12}| + |\lambda_{S21}|)^2 < \lambda_{S1} \lambda_{S2}. \quad (19)$$

Our benchmark points considered below satisfy these conditions.

The other four scalar potentials can formally be obtained from the Z_2 -invariant potential Eq. (3) by setting all the new terms added to V_c to zero, with the exception of the 1) λ'_S, μ_{SH} , 2) $\lambda'_S, \mu'_{SH}, 3) \mu'_S, \lambda'_S, \lambda''_S, \lambda'_{S1}, \lambda'_{S2}$, 4) $\mu'_S, \lambda'_S, \lambda''_S, \lambda'_{S1}, \lambda'_{S2}, \mu_{SH}, \mu'_{SH}$ terms.

The λ_5 term in potential (15) splits the down component of H_2 into two real scalar fields with different masses,

$$H_2 = \begin{pmatrix} -iH^+ \\ \frac{H^0 + iA^0}{\sqrt{2}} \end{pmatrix}. \quad (20)$$

Note that the complex scalar S does not mix with H_2 because these fields have different Z_N charges. As a result this model contains two dark sectors, the first one with the complex scalar S (the Z_4 charge is 1), the second one comprising the complex scalar H^+ and the real scalars H^0 and A^0 (the Z_4 charge is 2). Any of the neutral particles with a non-zero Z_4 charge can be a dark matter candidate. We will consider the masses of the neutral scalar particles, M_S, M_{H^0} and M_{A^0} , as independent parameters, then

$$\mu_S^2 = M_S^2 - \lambda_{S1} \frac{v^2}{2}, \quad (21)$$

$$\lambda_5 = \frac{M_{H^0}^2 - M_{A^0}^2}{v^2}, \quad (22)$$

$$\mu_2^2 = M_{H^0}^2 - (\lambda_3 + \lambda_4 + \lambda_5) \frac{v^2}{2}, \quad (23)$$

$$M_{H^+} = \sqrt{\frac{M_{A^0}^2 + M_{H^0}^2}{2} - \lambda_4 \frac{v^2}{2}}, \quad (24)$$

$$\lambda_1 = \frac{1}{2} \frac{M_h^2}{v^2}. \quad (25)$$

3 RELIC DENSITY IN CASE OF THE Z_3 SYMMETRY

3.1 Evolution equations

Consider the Z_3 -symmetric theory. The imposed Z_3 symmetry implies, as usual, just one dark matter candidate. This is because the Z_3 charges 1 and -1 correspond to a particle and its anti-particle. The new feature is that processes of the type $xx \rightarrow x^*X$, where X is any standard model particle, also contribute to dark matter annihilation. The equation for the number density reads

$$\frac{dn}{dt} = -\langle v\sigma^{xx^* \rightarrow XX} \rangle (n^2 - \bar{n}^2) - \frac{1}{2}\langle v\sigma^{xx \rightarrow x^*X} \rangle (n^2 - n\bar{n}) - 3Hn, \quad (26)$$

where we use $\bar{n} = n_{\text{eq}}$, H is the Hubble rate, and angular brackets mean thermal averaging. We define

$$\sigma_v \equiv \langle v\sigma^{xx^* \rightarrow XX} \rangle + \frac{1}{2}\langle v\sigma^{xx \rightarrow x^*X} \rangle \quad \text{and} \quad \alpha = \frac{1}{2} \frac{\sigma_v^{xx \rightarrow x^*X}}{\sigma_v}, \quad (27)$$

which means that $0 \leq \alpha \leq 1$. Here and in the following we use the notation, $\sigma_v^{xx \rightarrow x^*X} \equiv \langle v\sigma^{xx \rightarrow x^*X} \rangle$. In terms of the abundance, $Y = n/s$, where s is the entropy density, we obtain

$$\frac{dY}{dt} = -s\sigma_v \left(Y^2 - \alpha Y\bar{Y} - (1 - \alpha)\bar{Y}^2 \right) \quad (28)$$

or, using the entropy conservation condition $ds/dt = -3Hs$,

$$3H \frac{dY}{ds} = \sigma_v \left(Y^2 - \alpha Y\bar{Y} - (1 - \alpha)\bar{Y}^2 \right). \quad (29)$$

where $\bar{Y} = Y_{\text{eq}}$ is the equilibrium abundance. We use standard formulae for $H(T)$ and $s(T)$ [32] that allow to replace the entropy evolution with the temperature one. To solve this equation we follow the usual procedure [18, 32]. Writing $Y = \bar{Y} + \Delta Y$ we find the starting point for the numerical solution of this equation with the Runge-Kutta method using

$$3H \frac{d\bar{Y}}{ds} = \sigma_v \bar{Y} \Delta Y (2 - \alpha), \quad (30)$$

where $\Delta Y \ll Y$. This is similar to the standard case except that ΔY increases by a factor $1/(1 - \alpha/2)$. Furthermore, when solving numerically the evolution equation, the decoupling condition $Y^2 \gg \bar{Y}^2$ is modified to

$$Y^2 \gg \alpha Y\bar{Y} + (1 - \alpha)\bar{Y}^2. \quad (31)$$

This implies that the freeze-out starts at an earlier time and lasts until a later time as compared with the standard case. This modified evolution equation is implemented in micrOMEGAs [19, 33]. Although semi-annihilation processes can play a significant role in the computation of the relic density, the solution for the abundance depends only weakly on the parameter α , typically only by a few percent. This means in particular that the standard freeze-out approximation works with a good precision.

3.2 Numerical results with micrOMEGAs

Using the scalar potential defined in Eq. (4) we have implemented in micrOMEGAs the scalar model with a Z_3 symmetry. The scalar sector contains an additional scalar doublet and one complex singlet. The neutral component of the doublet mixes with the singlet, the lightest component x_1 is therefore the dark matter candidate, while the heavy component x_2 can decay into $x_1 h$, where h is the standard model-like Higgs boson. Because h can decay into light particles, x_2 is unstable even if the mass difference between x_1 and x_2 is small. Note that the doublet component of DM has a vector interaction

with the Z . This interaction is determined by the $SU(2) \times U(1)$ gauge group and leads to a large direct detection signal in conflict with exclusion limits, for example from XENON100 [34]. The only way to avoid this constraint is to consider a DM with a very small doublet component, namely we have to assume that the mixing angle

$$\theta \leq 0.025. \quad (32)$$

In the limit of small mixing, annihilation processes such as $x_1 x_1^* \rightarrow XX$ where X stands for W, Z, h , are dominated by the $\lambda_{S1}|S|^2|H_1|^2$ term. The semi-annihilation process $x_1 x_1 \rightarrow x_1^* h$ is mainly determined by a product of μ_S'' and λ_{S1} arising from the terms $\mu_S''(S^3 + S^{\dagger 3})/2$ and $\lambda_{S1}|S|^2|H_1|^2$ in Eq. 2 and Eq. 4. To illustrate a scenario where semi-annihilation channels contribute significantly and which predicts reasonable values for the relic density and the direct detection rate, we choose a benchmark point with the following parameters

λ_2	0.1	λ_S	0.2	λ_{S12}	0.1	M_{x_1}	150 GeV
λ_3	0.1	λ_{S1}	0.05	M_h	125 GeV	M_{x_2}	400 GeV
λ_4	0.1	λ_{S2}	0.1	μ_S''	80 GeV	$\sin \theta$	0.025

Table 2: Benchmark point for Z_3 .

For this point, the relic density is $\Omega h^2 = 0.105$. The dominant contribution to $(\Omega h^2)^{-1}$ is from semi-annihilation (54% for $x_1 x_1 \rightarrow h x_1^*$) while the annihilation channels $x_1 x_1^* \rightarrow WW, ZZ, hh$ give a relative contribution of 22%, 13% and 10% respectively. Fig. 1 illustrates the dependence of the relic density on the DM mass as compared to the relic density when semi-annihilation is ignored, $(\Omega h^2)_{\text{ann}}$. Here all other parameters are fixed to their benchmark values. When $M_{x_1} = 110$ GeV, semi-annihilation with a Higgs in the final state is kinematically forbidden at low velocities. If M_{x_1} increases, semi-annihilation plays an important role and Ωh^2 decreases rapidly due to the contribution of the channel $x_1 x_1 \rightarrow h x_1^*$. Note that $(\Omega h^2)_{\text{ann}}$ also decreases when M_{x_1} is such that the channel $x_1 x_1^* \rightarrow hh$ is allowed. When M_{x_1} approaches $M_{x_2}/2$, Ωh^2 falls again because the semi-annihilation channel is enhanced due to x_2 exchange near resonance.

The spin independent (SI) scattering cross section on nuclei as a function of the DM mass is illustrated in Fig. 1 (right panel). Here we average over dark matter and anti-dark matter cross sections assuming that they have the same density. The main contribution comes from the Z -exchange diagram because there is a $x_1 x_1^* Z$ coupling². Furthermore, one can easily show that the scattering amplitudes are not the same for protons and neutrons, with $f_p = (4 \sin^2 \theta_W - 1) f_n = -0.075 f_n$. Since the current experimental bounds on σ_{xp}^{SI} are extracted from experimental results assuming that the couplings to protons (f_p) and neutrons (f_n) are equal and the same as the couplings of x_1^* to protons (\bar{f}_p) and neutrons (\bar{f}_n), we define the normalised cross section on a point-like nucleus [35]:

$$\sigma_{xN}^{\text{SI}} = \frac{2}{\pi} \left(\frac{M_N M_{x_1}}{M_N + M_{x_1}} \right)^2 \left(\frac{[Z f_p + (A - Z) f_n]^2}{A^2} + \frac{[Z \bar{f}_p + (A - Z) \bar{f}_n]^2}{A^2} \right). \quad (33)$$

This quantity can directly be compared with the limit on σ_{xp}^{SI} .

²In the inert doublet model with a Z_2 symmetry [20, 22], a λ_5 term splits the complex doublet into a scalar and a pseudoscalar, when the mass splitting is small such coupling leads to inelastic scattering.

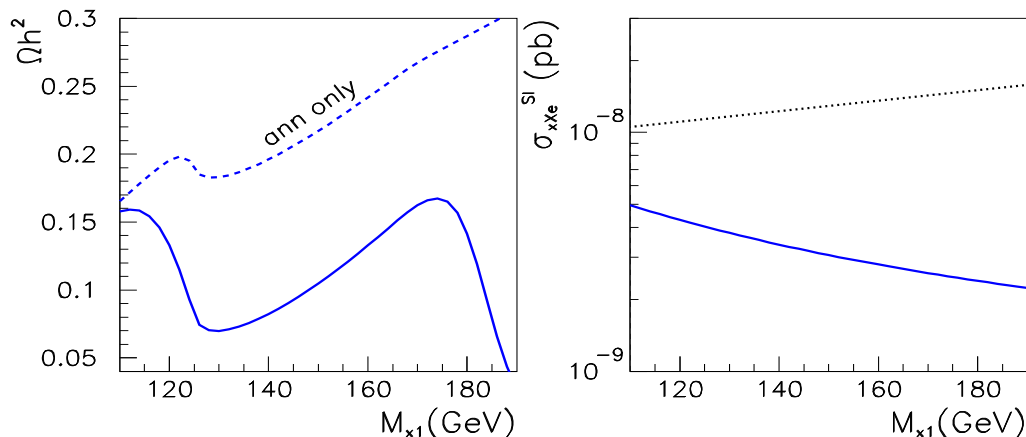


Figure 1: (Left panel) Ωh^2 as a function of the dark matter mass for the benchmark point with semi-annihilation (solid line), and without semi-annihilation (dashed). (Right panel) $\sigma_{x_1 X_e}^{\text{SI}}$ (solid). The experimental limit from XENON100 [34] is also displayed (dashed).

4 RELIC DENSITY IN CASE OF THE Z_4 SYMMETRY

4.1 Evolution equations

In the case of a Z_4 symmetry all particles can be divided into 3 classes³ $\{0,1,2\}$ according to the value of their Z_4 charges modulo 4. We can choose SM particles to have $X_{\text{SM}} = 0$. We will use the notation σ_v^{abcd} for the thermally averaged cross section for reactions $ab \rightarrow cd$ where $a, b, c, d = 0, 1, 2$ represent any particle with given X -charge. Let M_{x_1} and M_{x_2} be the masses of the lightest particles of classes 1 and 2 respectively. The lightest particle of class 1 is always stable and therefore a DM candidate. The lightest particle of class 2 is stable and can be a second DM candidate if $M_{x_2} < 2M_{x_1}$. Note that if $M_{x_2} > 2M_{x_1}$, then x_2 will decay before the freeze-out of x_1 and the relic density can be computed following the standard procedure.

The equations for the number density of particles 1 and 2 read

$$\frac{dn_1}{dt} = -\sigma_v^{1100} (n_1^2 - \bar{n}_1^2) - \sigma_v^{1120} \left(n_1^2 - \bar{n}_1^2 \frac{n_2}{\bar{n}_2} \right) - \sigma_v^{1122} \left(n_1^2 - n_2^2 \frac{\bar{n}_1^2}{\bar{n}_2^2} \right) - 3Hn_1, \quad (34)$$

$$\begin{aligned} \frac{dn_2}{dt} = & -\sigma_v^{2200} (n_2^2 - \bar{n}_2^2) + \frac{1}{2} \sigma_v^{1120} \left(n_1^2 - \bar{n}_1^2 \frac{n_2}{\bar{n}_2} \right) - \frac{1}{2} \sigma_v^{1210} (n_1 n_2 - n_1 \bar{n}_2) \\ & - \sigma_v^{2211} \left(n_2^2 - n_1^2 \frac{\bar{n}_2^2}{\bar{n}_1^2} \right) - 3Hn_2, \end{aligned} \quad (35)$$

where we use \bar{n}_i to designate the equilibrium number density of particle x_i . In σ_v^{abcd} all annihilation and coannihilation processes are taken into account. Here the semi-annihilation processes include all those, where 2 DM particles annihilate into one DM and one standard particle, specifically σ_v^{1120} and σ_v^{1210} . These two cross sections are also described by the same matrix element. However, there is no simple relation between these two cross sections because one process is in the s -channel and the other

³We take into account that $3 = -1 \pmod{4}$, so the particle with X -charge 3 is the antiparticle of a particle with X -charge 1.

in the t -channel. In terms of the abundance, $Y_i = n_i/s$,

$$3H \frac{dY_1}{ds} = \sigma_v^{1100} (Y_1^2 - \bar{Y}_1^2) + \sigma_v^{1120} \left(Y_1^2 - Y_2 \frac{\bar{Y}_1^2}{\bar{Y}_2} \right) + \sigma_v^{1122} \left(Y_1^2 - Y_2^2 \frac{\bar{Y}_1^2}{\bar{Y}_2^2} \right), \quad (36)$$

$$3H \frac{dY_2}{ds} = \sigma_v^{2200} (Y_2^2 - \bar{Y}_2^2) - \frac{1}{2} \sigma_v^{1120} \left(Y_1^2 - Y_2 \frac{\bar{Y}_1^2}{\bar{Y}_2} \right) + \frac{1}{2} \sigma_v^{1210} Y_1 (Y_2 - \bar{Y}_2) + \sigma_v^{2211} \left(Y_2^2 - Y_1^2 \frac{\bar{Y}_2^2}{\bar{Y}_1^2} \right). \quad (37)$$

Solving these equations we use standard formulas for entropy $s(T)$ and the Hubble rate $H(T)$ temperature dependence [32] that allow to replace the dependence on entropy with one on temperature. The thermally averaged cross section involving particles of different sectors can be expressed as

$$\sigma_v^{IJKL}(T) = \frac{T}{64\pi^5 s^2 \bar{Y}_I(T) \bar{Y}_J(T)} \int \frac{ds}{\sqrt{s}} K_1 \left(\frac{\sqrt{s}}{T} \right) p_{\text{in}} p_{\text{out}} \sum_{\substack{a \in I \\ c \in K \\ \text{pol.}}} \int_{-1}^1 |\mathcal{M}_{ab \rightarrow cd}(\sqrt{s}, \cos \Theta)|^2 d \cos \theta, \quad (38)$$

$$\bar{Y}_I(T) = \frac{T}{2\pi^2 s} \sum_{i \in I} g_i m_i^2 K_2 \left(\frac{m_i}{T} \right), \quad (39)$$

where $\mathcal{M}_{ab \rightarrow cd}$ is the matrix element for the $2 \rightarrow 2$ process and K_1, K_2 are modified Bessel functions of the second kind. For reactions which are kinematically open at zero relative velocity, σ_v depends slowly on temperature. Otherwise there is a strong $\exp(-\Delta M/T)$ temperature dependence, where ΔM is the difference between the sums of the masses of outgoing and incoming particles. Equation (38) leads to relations between different cross sections

$$Y_I Y_J \sigma_v^{IJKL} = Y_K Y_L \sigma_v^{KLJI}. \quad (40)$$

In particular it implies that, $\sigma_v^{0211} = \sigma_v^{1120} Y_1^2 / Y_2$, where the abundance of incoming SM particles $Y_0 = 1$.

Introducing $\Delta Y_i = Y_i - \bar{Y}_i$, Eqs. (36) and (37) take a simple form

$$3H \frac{\Delta Y_i}{ds} = -C_i + A_{ij}(T) \Delta Y_j + Q_{ijk}(T) \Delta Y_j \Delta Y_k, \quad (41)$$

where

$$C_i = 3H \frac{d\bar{Y}_i}{ds}, \quad (42)$$

$$A = \begin{pmatrix} 2(\sigma_v^{1100} + \sigma_v^{1122} + \sigma_v^{1120})\bar{Y}_1 & -(\sigma_v^{1120} + 2\sigma_v^{1122})\frac{\bar{Y}_1^2}{\bar{Y}_2} \\ -\sigma_v^{1120}\bar{Y}_1 - 2\sigma_v^{1122}\bar{Y}_1 & 2(\sigma_v^{2200} + \sigma_v^{2211})\bar{Y}_2 + 0.5(\sigma_v^{1210} + \sigma_v^{1120}\frac{\bar{Y}_1}{\bar{Y}_2})\bar{Y}_1 \end{pmatrix}, \quad (43)$$

$$Q_1 = \begin{pmatrix} \sigma_v^{1100} + \sigma_v^{1122} + \sigma_v^{1120} & 0 \\ 0 & -\sigma_v^{2211} \end{pmatrix}, \quad (44)$$

$$Q_2 = \begin{pmatrix} -\sigma_v^{1120} - \sigma_v^{1122} & \frac{1}{2}\sigma_v^{1210} \\ 0 & \sigma_v^{2200} + \sigma_v^{2211} \end{pmatrix}. \quad (45)$$

$$(46)$$

At large temperatures we expect the densities of both DM components to be close to their equilibrium values. In general in micrOMEGAs [36] the equation for the abundance is solved numerically starting from large temperatures. However, this procedure poses a problem for Eq. (41). The step of the numerical solution is inversely proportional to $A(T)$ and as long as $A(T)$ is not suppressed by the Boltzmann factor included in \bar{Y} , the step is too small and the numerical method fails.

To avoid this problem, we use the fact that at large temperatures one can neglect the Q term in Eq. (41) and write the explicit solution for the linearised equation. The approximate solution in the case of large A is

$$\Delta Y_i(s) = A_{ij}^{-1}(s)C_j(s). \quad (47)$$

One can use Eq. (47) to find the lowest temperature where $\Delta Y_i \approx 0.05Y_i$ and start solving numerically Eq. (41) from this temperature. In the general case it gives a reasonable step for the numerical solution $\delta s/s \approx 0.1$, where s is the variable of integration. This method can, however, lead to some numerical problems if the masses of the two dark matter particles are very different. Let us call the light particle l and the heavy particle h . We have to start the numerical solution at a temperature T above the freeze-out temperature of the heaviest DM,

$$T_{\text{fo}h} \approx M_h/25. \quad (48)$$

At this temperature,

$$\frac{Y_l}{Y_h} \approx \exp \frac{M_h - M_l}{T_{\text{fo}h}}, \quad (49)$$

and the step in the numerical solution of the two component equations will be suppressed by a factor $\exp(-M_h - M_l)/T_{\text{fo}h}$. This small step size is problematic when solving numerically the equation with the Runge-Kutta method. This occurs when $M_h/M_l > 2$. In this case the equation for the heavy component must be solved independently assuming that the light component has reached its equilibrium density. If $M_h/M_l < 2$, the Runge-Kutta procedure can be used to successfully solve the thermal evolution equations (41).

The abundances Y_1 and Y_2 will be modified by the interactions between the two dark matter sectors.⁴ Thus the new terms in Eq. (36) will simply add to the standard annihilation process with SM particles and will contribute to decrease the final abundance Y_1 . After x_2 freezes-out, interactions of the type $22 \rightarrow 11$ lead to an increase of Y_2 . When $M_{x_1} \ll M_{x_2}$, the evolution of Y_2 will be strongly influenced by the first sector since at its freeze-out temperature Y_1 is large. Following the same argument as above the new annihilation terms in Eq. (37) will contribute to a decrease in the final abundance Y_2 . Furthermore, the semi-annihilation process $12 \rightarrow 10$ which is always kinematically open means that x_1 acts as a catalyst for the transformation of x_2 into SM particles. Thus the light component forces the heavy one to keep its equilibrium value, resulting in a significant decrease of the relic density of x_2 . When both DM particles have similar masses, the interplay between the two sectors is more complicated, in particular the rôle of the interactions of the type $20 \rightarrow 11$ will depend on the exact mass relation between the two DM particles. For example, this interaction can lead to an increase of the abundance of x_2 if Y_1 is large enough for the reverse process to give the largest contribution.

4.2 Numerical results

The scalar model with a Z_4 symmetry contains two dark sectors. In sector 1 the DM candidate is a complex singlet, S , the main contribution to σ_v^{1100} comes from annihilation into Higgs pairs and is determined by the term $\lambda_{S1}|S|^2|H_1|^2$. Sector 2 is similar to the Inert Doublet Model (IDM). The DM candidate can be either the scalar H^0 or the pseudoscalar A^0 . Annihilation of DM into SM particles is

⁴Note that Y_1 and Y_2 correspond to the abundances of the particles with a given Z_4 charge. The relative size of the masses of the DM particles depend on the choice of parameters in a given model.

usually dominated by gauge boson pair production processes, while annihilation into fermion pairs as well as co-annihilation processes can also contribute. Furthermore, for a DM mass at the electroweak scale, it was shown in [37] that annihilation into 3-body final states via a virtual W can be important below the W threshold. To avoid this complication we will consider a DM with a mass above masses of the W , Z , and h . Under this condition, the DM annihilation into SM particles in sector 2 is driven by $SU(2) \times U(1)$ gauge interactions and leads typically to a value of $\Omega h^2 < 0.1$, except for a DM heavier than about 500 GeV. The co-annihilation of H^0 , A^0 , H^\pm states increases Ωh^2 .

We will consider a benchmark point where both DM candidates S and H^0 have a mass near 350 GeV. Other parameters are chosen so that semi-annihilation processes play an important role, while both components have comparable relic density and $\Omega h^2 = \Omega_1 h^2 + \Omega_2 h^2 = 0.1$. In particular to have $\Omega_2 h^2 \approx 0.05$ requires the contribution of coannihilation processes – we therefore impose a small mass splitting $M_{H^0} \approx M_{A^0}$, meaning that λ_5 will be small, see Eq. (22). Furthermore, a small value of λ_4 also leads to a small mass splitting with the charged Higgs. Note that for small λ_5 and λ_4 the positivity condition on the potential, Eqs. (2,15) is easily satisfied.

λ_2	0.1	λ_{S1}	0.1	λ'_S	0.1	M_A	341 GeV
λ_3	0.1	λ_{S2}	0.3	μ_S	100 GeV	M_H	339 GeV
λ_4	0.01	λ_{S12}	0.13	M_h	125 GeV	M_S	350 GeV
λ_5	0.1	λ_{S21}	0.13				

Table 3: Benchmark point for Z_4 .

The results of the calculation of the relic density when including different terms in Eq. (36,37) is presented in Table 4. When only (co-)annihilation into SM particles are taken into account, the relic density of S is too high, while annihilation is much more efficient in Sector 2. Adding the interactions of the type of $1, 1 \leftrightarrow 2, 2$ brings the value of $\Omega_1 h^2$ and $\Omega_2 h^2$ closer to each other. In our example the DM in sector 1 has weak interactions with SM particles, therefore $\Omega_1 h^2$ is large when sector 2 is neglected. As a result of interactions with sector 2 particles the value for $\Omega_1 h^2$ is significantly reduced. This effect was also observed for a DM model with a $Z_2 \times Z_2$ symmetry [17] and was called the *assisted freeze-out mechanism*. Finally, when semi-annihilation processes are included, both $\Omega_1 h^2$ and $\Omega_2 h^2$ decrease. Note that for this benchmark point, the cross section for DM elastic scattering on proton

included terms of Eq(36,37)	$\Omega_1 h^2$	$\Omega_2 h^2$
$\sigma_v^{1100}, \sigma_v^{2200}$	0.24	0.041
$\sigma_v^{1100}, \sigma_v^{2200}$ and σ_v^{1122}	0.079	0.064
All	0.050	0.051

Table 4: Relic density of DM particles for the Z_4 benchmark point.

and neutron is $1.5(1.8) \cdot 10^{-9}$ pb for the DM in sector 1 and 2, respectively. This is well below current exclusion limits of XENON100 [34], as will be discussed at the end of this section.

To examine more closely the interplay between the two DM sectors as well as the role of semi-annihilation in determining the DM abundance, we let M_S vary in the range 200-600 GeV and solve for the relic density by including new terms one by one. All other parameters are fixed to the value for the benchmark in Table 3.

First we consider only the impact of annihilation processes, the results are displayed in Fig. 2 (left). When solving the evolution equation for the two DM independently, $\Omega_1 h^2$ rises rapidly with M_S while $\Omega_2 h^2$ remains constant. Note that for the model under consideration we have that $\sigma_v^{1100} < \sigma_v^{2200}$ hence

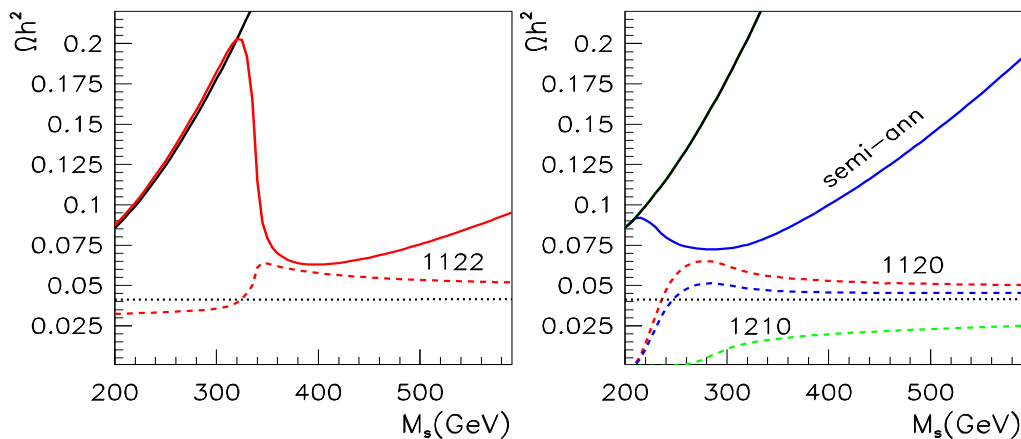


Figure 2: Effect of interactions between the two dark matter sectors (left) and of semi-annihilation (right) on $\Omega_1 h^2$ (solid) and $\Omega_2 h^2$ (dashed) as a function of M_S . Left panel – Including only σ_v^{1100} and σ_v^{2200} (black) as well as σ_v^{1122} , σ_v^{2211} (red). Right panel – Including only σ_v^{1210} (green), only σ_v^{1120} (red) as well as all semi-annihilations (blue), as a reference in black $\Omega_1 h^2$ (solid) and $\Omega_2 h^2$ (dot) with only standard annihilation terms. Note that σ_v^{1210} does not change $\Omega_1 h^2$.

$\Omega_1 h^2 > \Omega_2 h^2$. The impact of σ_v^{1122} and σ_v^{2211} on the relic density depends on the relative masses of the scalar and doublet DM. The heavier DM candidate freezes out at a larger temperature than the lighter one, $T_{\text{fo}h} > T_{\text{fo}l}$. If the mass difference is large, this happens when the light one is at its equilibrium value. Thus the contribution of σ_v^{hhll} just adds to σ_v^{hh00} , leading to a decrease of the heavy DM abundance. Furthermore, after the light DM freezes out, interactions such as $hh \rightarrow ll$ give an additional source of light DM, while the reverse reaction is suppressed by a Boltzmann factor. This effect can, however, be small when the heavy particles have a low density at this point. Thus the interactions between DM sectors 1 and 2 lead altogether to a decrease of the abundance of the heavy component and an increase of the light component. This is observed in the left panel of Fig. 2. In the region where $M_S < M_{H^0} = 350$ GeV, $\Omega_2 h^2$ decreases while in the region $M_S > M_{H^0}$, $\Omega_2 h^2$ increases and vice-versa for $\Omega_1 h^2$. Note that for large values of M_S , interactions with SM particles are weak so $\sigma_v^{1122} \gg \sigma_v^{1100}$, leading to a large decrease in $\Omega_1 h^2$. When there is a small difference between the two DM particles, the freeze-out temperatures of both component are similar. The density of the heavy DM component has not yet decreased to its final value at the time the light component freezes out, thus the effect of $hh \leftrightarrow ll$ interactions in increasing the abundance of the light component is more important. This is particularly noticeable when looking at the curve for $\Omega_2 h^2$ in the region, where M_S is just above $M_{H^0} = 350$ GeV in Fig. 2 (left). This discussion, where we ignore the semi-annihilation terms, applies to models with $\lambda_{S12} = \lambda_{S21} = 0$. In this case the Z_4 symmetry is replaced with a $Z_2 \times Z_2$ symmetry.

Next we consider the impact of semi-annihilation processes, ignoring the annihilation of pairs of particles from sector 1 to 2. The σ_v^{1210} term does not affect $\Omega_1 h^2$ and works as a catalyst for $2 \rightarrow \text{SM}$ transitions. This term has an effect only after the freeze-out of H^0 and its effect is stronger when Y_1 is large, see Eq. (37). Thus in the region $M_S > M_{H^0}$ where the freeze-out of S occurs first (at a higher temperature), we find a roughly constant factor of suppression of $\Omega_2 h^2$. As M_S decreases, its abundance Y_1 at the freeze-out of H^0 ($T_{\text{fo}h}$) will increase, thus the suppression of $\Omega_2 h^2$ is more important, see Fig. 2. Note that the suppression of $\Omega_2 h^2$ for $M_S > M_{H^0}$ is significantly larger than for the other semi-annihilation processes that we will discuss below. This is because the σ_v^{1210} term in

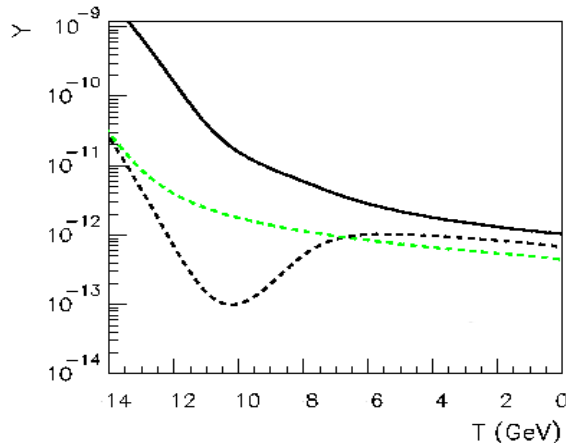


Figure 3: Temperature evolution of Y_1 (solid) and Y_2 (dashed) with standard terms and the contribution of σ_v^{1120} for $M_S = 260$ GeV. Temperature evolution of Y_2 with only standard terms (green/dashed), T is in GeV.

Eq. 37 depends on Y_1^2 , which is large in this approximation.

The second type of semi-annihilation process, $11 \rightarrow 20$ (or its reverse $20 \rightarrow 11$) leads to variations in the relic density of both DM components. If $M_S > M_{H^0}$, the impact of σ_v^{1120} is very similar to the one discussed above for σ_v^{1122} . For S , the heavy component, the overall annihilation cross section is increased, leading to a decrease in Ω_1 , illustrated by the blue curve in Fig. 2. For H^0 , the relic density increases because the process $11 \rightarrow 20$ is an additional source of sector 2 particles. This increase is even more important when both particles have similar masses – see the blue dashed curve in Fig. 2 when $M_S = 260$ -350 GeV. To examine more closely the impact of the semi-annihilation in the region where the mass of both DM particles are similar, we compute the temperature evolution of Y_1 and Y_2 choosing $M_S = 260$ GeV. The result is displayed in Fig. 3, in particular comparing the evolution of Y_2 with and without the contribution of σ_v^{1120} . For this choice of masses, the freeze-out of H^0 occurs when the abundance $Y_1 = \bar{Y}_1$ is large, this means that the term

$$-\frac{1}{2}\sigma_v^{1120}\left(Y_1^2 - \frac{Y_2\bar{Y}_1^2}{\bar{Y}_2}\right) = +\frac{1}{2}\sigma_v^{1120}\bar{Y}_1^2\left(\frac{Y_2}{\bar{Y}_2} - 1\right)\dots \quad (50)$$

in Eq. (37) forces Y_2 to follow its equilibrium value. Thus Y_2 is further reduced by semi-annihilation at large temperatures. After the freeze-out of S , when $Y_1 \gg \bar{Y}_1$, the same interaction leads to an increase of Y_2 . Thus the overall effect is an increase in the abundance of class 2 particles as compared with the case where only standard interactions are considered.

Finally, when $M_S < 260$ GeV, the cross section σ_v^{1120} , which consists of processes of the type $SS \rightarrow H^0 h$ is small because of a lack of phase space, thus $\Omega_1 h^2$ is the same as when only standard annihilation terms were included. At the same time the reverse process, $20 \rightarrow 11$ drives the depletion of class 2 particles and $\Omega_2 h^2$ drops to very small values. Note that when $M_{H^0} > 2M_S$ we expect that the class 2 DM will decay into pairs of class 1 particles since they are allowed by the Z_4 symmetry. However, in this example, the effect of σ_v^{1210} and σ_v^{1120} terms already leads to very small values of $\Omega_2 h^2$ for low values of M_S , so that the decays are irrelevant. In summary, the combined effect of semi-annihilation processes is for this example close to the result of only including σ_v^{1120} , see Fig. 2.

The result for $\Omega_1 h^2$ and $\Omega_2 h^2$ including all annihilation and semi-annihilation processes is displayed in Fig. 4. The semi-annihilation mechanisms dominate for $M_S < M_{H^0}$ while the assisted freeze-out

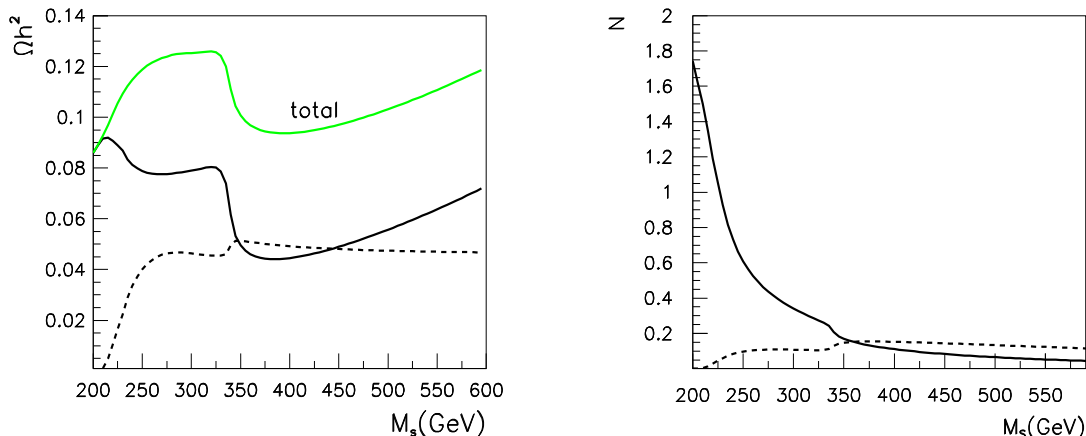


Figure 4: Left: $\Omega_1 h^2$ (solid), $\Omega_2 h^2$ (dashed) and Ωh^2 (green) as a function of M_S , the singlet DM mass. Right: Number of events expected in XENON100 from S (solid) and H^0 (dashed) elastic scattering as a function of M_S .

mechanism is the dominant effect when $M_S > M_{H^0}$. The total dark matter abundance is within about 10% of the value preferred by WMAP measurements over the whole range of masses considered. While the features we have described here are generic, the relative importance of different annihilation and semi-annihilation processes is model dependent and depends on the size of the various cross sections within a specific model.

Finally we compute the spin-independent cross section for S and H^0 scattering on xenon nuclei. As mentioned above at the benchmark point $\sigma^{\text{SI}} = 1.5(1.8) \times 10^{-9}$ pb for the DM in sector 1 and 2 respectively. We then compute the number of events that should be expected in XENON100 [34] in the interval $8.4 \text{ keV} < E < 44.6 \text{ keV}$ after an exposure of $1171 \text{ kg}\cdot\text{day}$. The number of events is directly proportional to the DM local density and we assume that the fraction of each DM component locally is the same as in the early universe, $\rho_i = \rho \Omega_i / \Omega_{\text{tot}}$ where $\rho = 0.3$. For S the cross section is largest for small masses, furthermore S contributes maximally to the DM density, hence the maximum predicted number of events, see Fig. 4. The cross section for H^0 scattering on nuclei is clearly independent of M_S , the variation of the number of events is simply due to the variation in the density of the second DM.

5 CONCLUSIONS

We have formulated scalar dark matter models with the minimal particle content in which dark matter stability is due to the discrete Z_N symmetry with $N > 2$. Already the minimal models containing one extra scalar singlet and doublet possess non-trivial dark matter phenomenology. In particular, the annihilation processes with new topologies like $x_i x_j \rightarrow x_k X$, where x_i is one of the dark matter particles and X is any standard model particle, change the dark matter freeze-out process and must be taken into account when calculating the dark matter relic abundance. Furthermore, in models with two dark matter candidates, annihilation processes involving only particles of two different dark matter sectors also impact the relic abundance of both dark matter particles. We have performed an example study of semi-annihilations in two scalar dark matter models based on Z_3 and Z_4 symmetries. We implemented those models for micrOMEGAs and studied the impact of semi-annihilations and

of the interactions between the dark sectors on the generation of dark matter relic abundance at the early Universe and the predictions for dark matter direct detection relevant for the presently running XENON100 experiment. We conclude that in this type of models both semi-annihilations and dark sector interactions may significantly affect the dark matter phenomenology compared to the well studied Z_2 models, and, therefore, must be taken into account in precise numerical analyses of dark matter properties.

ACKNOWLEDGEMENTS

Part of this work was performed in the Les Houches 2011 *Physics at TeV colliders* Workshop. K.K. and M.R. were supported by the ESF grants 8090, 8499, 8943, MTT8, MTT59, MTT60, MJD140, by the recurrent financing SF0690030s09 project and by the European Union through the European Regional Development Fund. A.P. was supported by the Russian foundation for Basic Research, grant RFBR-10-02-01443-a. The work of A.P. and G.B. was supported in part by the GDRI-ACPP of CNRS.

References

- [1] G. R. Farrar and P. Fayet, *Phenomenology of the Production, Decay, and Detection of New Hadronic States Associated with Supersymmetry*, *Phys.Lett.* **B76** (1978) 575–579.
- [2] L. M. Krauss and F. Wilczek, *Discrete Gauge Symmetry in Continuum Theories*, *Phys.Rev.Lett.* **62** (1989) 1221.
- [3] H. Fritzsch and P. Minkowski, *Unified Interactions of Leptons and Hadrons*, *Annals Phys.* **93** (1975) 193–266.
- [4] S. P. Martin, *Some simple criteria for gauged R-parity*, *Phys.Rev.* **D46** (1992) 2769–2772, [[hep-ph/9207218](#)].
- [5] M. Kadastik, K. Kannike, and M. Raidal, *Matter parity as the origin of scalar Dark Matter*, *Phys.Rev.* **D81** (2010) 015002, [[arXiv:0903.2475](#)].
- [6] M. Kadastik, K. Kannike, and M. Raidal, *Dark Matter as the signal of Grand Unification*, *Phys.Rev.* **D80** (2009) 085020, [[arXiv:0907.1894](#)].
- [7] L. E. Ibanez and G. G. Ross, *Discrete gauge symmetry anomalies*, *Phys.Lett.* **B260** (1991) 291–295.
- [8] K. Agashe and G. Servant, *Warped unification, proton stability and dark matter*, *Phys.Rev.Lett.* **93** (2004) 231805, [[hep-ph/0403143](#)].
- [9] K. Agashe and G. Servant, *Baryon number in warped GUTs: Model building and (dark matter related) phenomenology*, *JCAP* **0502** (2005) 002, [[hep-ph/0411254](#)].
- [10] H. K. Dreiner, C. Luhn, and M. Thormeier, *What is the discrete gauge symmetry of the MSSM?*, *Phys.Rev.* **D73** (2006) 075007, [[hep-ph/0512163](#)].
- [11] E. Ma, *$Z(3)$ Dark Matter and Two-Loop Neutrino Mass*, *Phys.Lett.* **B662** (2008) 49–52, [[arXiv:0708.3371](#)].
- [12] K. Agashe, D. Kim, M. Toharia, and D. G. Walker, *Distinguishing Dark Matter Stabilization Symmetries Using Multiple Kinematic Edges and Cusps*, *Phys.Rev.* **D82** (2010) 015007, [[arXiv:1003.0899](#)].

- [13] K. Agashe, D. Kim, D. G. Walker, and L. Zhu, *Using M_{T2} to Distinguish Dark Matter Stabilization Symmetries*, *Phys.Rev.* **D84** (2011) 055020, [arXiv:1012.4460].
- [14] B. Batell, *Dark Discrete Gauge Symmetries*, *Phys.Rev.* **D83** (2011) 035006, [arXiv:1007.0045].
- [15] F. D’Eramo and J. Thaler, *Semi-annihilation of Dark Matter*, *JHEP* **1006** (2010) 109, [arXiv:1003.5912].
- [16] Z.-P. Liu, Y.-L. Wu, and Y.-F. Zhou, *Enhancement of dark matter relic density from the late time dark matter conversions*, *Eur.Phys.J.* **C71** (2011) 1749, [arXiv:1101.4148].
- [17] G. Belanger and J.-C. Park, *Assisted freeze-out*, arXiv:1112.4491.
- [18] G. Belanger, F. Boudjema, A. Pukhov, and A. Semenov, *micrOMEGAs: Version 1.3*, *Comput.Phys.Commun.* **174** (2006) 577–604, [hep-ph/0405253].
- [19] G. Belanger, F. Boudjema, A. Pukhov, and A. Semenov, *MicrOMEGAs 2.0: A Program to calculate the relic density of dark matter in a generic model*, *Comput.Phys.Commun.* **176** (2007) 367–382, [hep-ph/0607059].
- [20] N. G. Deshpande and E. Ma, *Pattern of Symmetry Breaking with Two Higgs Doublets*, *Phys.Rev.* **D18** (1978) 2574.
- [21] E. Ma, *Verifiable radiative seesaw mechanism of neutrino mass and dark matter*, *Phys.Rev.* **D73** (2006) 077301, [hep-ph/0601225].
- [22] R. Barbieri, L. J. Hall, and V. S. Rychkov, *Improved naturalness with a heavy Higgs: An Alternative road to LHC physics*, *Phys.Rev.* **D74** (2006) 015007, [hep-ph/0603188].
- [23] L. Lopez Honorez, E. Nezri, J. F. Oliver, and M. H. Tytgat, *The Inert Doublet Model: An Archetype for Dark Matter*, *JCAP* **0702** (2007) 028, [hep-ph/0612275].
- [24] J. McDonald, *Gauge Singlet Scalars as Cold Dark Matter*, *Phys. Rev.* **D50** (1994) 3637–3649, [hep-ph/0702143].
- [25] V. Barger, P. Langacker, M. McCaskey, M. J. Ramsey-Musolf, and G. Shaughnessy, *LHC Phenomenology of an Extended Standard Model with a Real Scalar Singlet*, *Phys. Rev.* **D77** (2008) 035005, [arXiv:0706.4311].
- [26] V. Barger, P. Langacker, M. McCaskey, M. Ramsey-Musolf, and G. Shaughnessy, *Complex Singlet Extension of the Standard Model*, *Phys. Rev.* **D79** (2009) 015018, [arXiv:0811.0393].
- [27] C. P. Burgess, M. Pospelov, and T. ter Veldhuis, *The minimal model of nonbaryonic dark matter: A singlet scalar*, *Nucl. Phys.* **B619** (2001) 709–728, [hep-ph/0011335].
- [28] M. Gonderinger, Y. Li, H. Patel, and M. J. Ramsey-Musolf, *Vacuum Stability, Perturbativity, and Scalar Singlet Dark Matter*, *JHEP* **1001** (2010) 053, [arXiv:0910.3167].
- [29] M. Kadastik, K. Kannike, A. Racioppi, and M. Raidal, *EWSB from the soft portal into Dark Matter and prediction for direct detection*, *Phys.Rev.Lett.* **104** (2010) 201301, [arXiv:0912.2729].
- [30] M. Kadastik, K. Kannike, A. Racioppi, and M. Raidal, *Implications of the CDMS result on Dark Matter and LHC physics*, *Phys.Lett.* **B694** (2010) 242–245, [arXiv:0912.3797].
- [31] K. Huitu, K. Kannike, A. Racioppi, and M. Raidal, *Long-lived charged Higgs at LHC as a probe of scalar Dark Matter*, *JHEP* **1101** (2011) 010, [arXiv:1005.4409].

- [32] P. Gondolo and G. Gelmini, *Cosmic abundances of stable particles: Improved analysis*, *Nucl.Phys.* **B360** (1991) 145–179.
- [33] G. Belanger, F. Boudjema, P. Brun, A. Pukhov, S. Rosier-Lees, *et. al.*, *Indirect search for dark matter with micrOMEGAs2.4*, *Comput.Phys.Commun.* **182** (2011) 842–856, [[arXiv:1004.1092](#)].
- [34] **XENON100 Collaboration** Collaboration, E. Aprile *et. al.*, *Dark Matter Results from 100 Live Days of XENON100 Data*, *Phys.Rev.Lett.* **107** (2011) 131302, [[arXiv:1104.2549](#)].
- [35] G. Belanger, M. Kakizaki, E. Park, S. Kraml, and A. Pukhov, *Light mixed sneutrinos as thermal dark matter*, *JCAP* **1011** (2010) 017, [[arXiv:1008.0580](#)].
- [36] G. Belanger, F. Boudjema, A. Pukhov, and A. Semenov, *MicrOMEGAs: A Program for calculating the relic density in the MSSM*, *Comput.Phys.Commun.* **149** (2002) 103–120, [[hep-ph/0112278](#)].
- [37] C. E. Yaguna, *Large contributions to dark matter annihilation from three-body final states*, *Phys.Rev.* **D81** (2010) 075024, [[arXiv:1003.2730](#)].